Journal of Computational Physics 228 (2009) 7941–7956

Contents lists available at ScienceDirect

Journal of Computational Physics

journal homepage: www.elsevier.com/locate/jcp

A minimal energy tracking method for non-radially symmetric solutions of coupled nonlinear Schrödinger equations

Yueh-Cheng Kuo [a], Wen-Wei Lin [b], Shih-Feng Shieh [c], Weichung Wang [d,*]

[a] Department of Applied Mathematics, National University of Kaohsiung, Kaohsiung 811, Taiwan
[b] Department of Applied Mathematics, National Chiao-Tung University, Hsinchu 300, Taiwan
[c] Department of Mathematics, National Taiwan Normal University, Taipei 116, Taiwan
[d] Department of Mathematics, National Taiwan University, Taipei 106, Taiwan

ARTICLE INFO

Article history:
Received 19 February 2009
Received in revised form 4 July 2009
Accepted 18 July 2009
Available online 3 August 2009

Keywords:
Coupled nonlinear Schrödinger equations
Continuation method
Ground states
Minimal energy
Non-radially symmetric solutions

ABSTRACT

We aim at developing methods to track minimal energy solutions of time-independent m-component coupled discrete nonlinear Schrödinger (DNLS) equations. We first propose a method to find energy minimizers of the 1-component DNLS equation and use it as the initial point of the m-component DNLS equations in a continuation scheme. We then show that the change of local optimality occurs only at the bifurcation points. The fact leads to a minimal energy tracking method that guides the choice of bifurcation branch corresponding to the minimal energy solution curve. By combining all these techniques with a parameter-switching scheme, we successfully compute a non-radially symmetric energy minimizer that can not be computed by existing numerical schemes straightforwardly.

1. Introduction

The main theme of this article is to compute the energy minimizers of m-component coupled discrete nonlinear Schrödinger equations. We consider the time-dependent m-component nonlinear Schrödinger (NLS) equations that are defined as

$$-\iota\frac{\partial}{\partial t}\Phi_j = [\triangle - V(\mathbf{z})]\Phi_j + \mu_j|\Phi_j|^2\Phi_j + \sum_{i\neq j, i=1}^{m}\beta_{ij}|\Phi_i|^2\Phi_j, \tag{1a}$$

$$\Phi_j = \Phi_j(t,\mathbf{z}) \in \mathbb{C},\ \mathbf{z}\in\Omega\subseteq\mathbb{R}^n,\quad j=1,\ldots,m, \tag{1b}$$

$$\Phi_j(t,\mathbf{z}) = 0,\ \text{as}\ \mathbf{z}\in\partial\Omega, \tag{1c}$$

where the μ_j are positive constants, $n\leqslant 3, V(\mathbf{z})>0$ and $\beta_{ij}=\beta_{ji}(i\neq j)$ are coupling coefficients. If $\Omega=\mathbb{R}^n$, the boundary condition (1c) becomes

$$\Phi_j(t,\mathbf{z})\to 0,\ \text{as}\ |\mathbf{z}|\to\infty,\quad t>0.$$

To obtain the solitary wave solutions, we set $\Phi_j(t,\mathbf{z}) = e^{-\iota\lambda_j t}\phi_j(\mathbf{z})$ and transform (1) into the time-independent m-component NLS equations

* Corresponding author. Tel.: +886 2 33662871; fax: +886 2 2391 4439.
E-mail addresses: yckuo@nuk.edu.tw (Y.-C. Kuo), wwlin@math.nctu.edu.tw (W.-W. Lin), sfshieh@math.ntnu.edu.tw (S.-F. Shieh), wwang@math.ntu.edu.tw (W. Wang).

0021-9991/$ - see front matter © 2009 Elsevier Inc. All rights reserved.
doi:10.1016/j.jcp.2009.07.029

$$[\triangle - V(\mathbf{z})]\phi_j - \lambda_j\phi_j + \mu_j|\phi_j|^2\phi_j + \sum_{i\neq j, i=1}^{m}\beta_{ij}|\phi_i|^2\phi_j = 0, \text{ in } \mathbb{R}^n, \tag{2a}$$

$$\phi_j > 0 \text{ in } \Omega \subseteq \mathbb{R}^n, \quad j = 1,\ldots,m, \tag{2b}$$

$$\phi_j(\mathbf{z}) = 0, \text{ as } \mathbf{z} \in \partial\Omega. \tag{2c}$$

To solve Eqs. (2) numerically, we consider the corresponding m-component discrete nonlinear Schrödinger (DNLS) equations

$$\begin{cases} \mathbf{A}\mathbf{u}_j - \lambda_j\mathbf{u}_j + \mu_j\mathbf{u}_j^{②}\circ\mathbf{u}_j + \sum_{i\neq j, i=1}^{m}\beta_{ij}\mathbf{u}_i^{②}\circ\mathbf{u}_j = \mathbf{0}, \\ \mathbf{u}_j > 0, \ \mathbf{u}_j \in \mathbb{R}^N, \ \text{for } j = 1,\ldots,m, \end{cases} \tag{3}$$

where $\mathbf{u}_j \in \mathbb{R}^N$ denotes the approximation of $\phi_j(\mathbf{z})$, for $j = 1,\ldots,m$. Here $\mathbf{A} \in \mathbb{R}^{N\times N}$ is the standard central finite difference discretization matrix of the operator $[\triangle - V(\mathbf{z})]$ with the homogeneous Dirichlet boundary conditions on a finite domain $\Omega \subseteq \mathbb{R}^n$, with $\mathbf{u}_j|_{\partial\Omega} = 0$. In addition, $\mathbf{A}$ is an irreducible and symmetric negative definite matrix. The size of N depends on the approximation domain and grid sizes. For example, if a uniform grid size h is applied over a two-dimensional finite domain $[-d,d]\times[-d,d]$ and $\left(\frac{2d}{h}-1\right)$ is a positive integer, we have a $N = \left(\frac{2d}{h}-1\right)^2$. For $\mathbf{u} = (u_1,\ldots,u_N)^\top, \mathbf{v} = (v_1,\ldots,v_N)^\top \in \mathbb{R}^N, \mathbf{u}\circ\mathbf{v} = (u_1v_1,\ldots,u_Nv_N)^\top$ denotes the Hadamard product of $\mathbf{u}$ and $\mathbf{v}$ and $\mathbf{u}^{②} = \mathbf{u}\circ\cdots\circ\mathbf{u}$ denotes the r-time Hadamard product of $\mathbf{u}$.

The NLS Eqs. (1) model a physical phenomenon in nonlinear optics [1], where the solution Φ_j denotes the jth component of the beam in Kerr-like photorefractive media. The positive constant μ_j measures the self-focusing in the jth component of the beam; and λ_j is the chemical potential. The coupling coefficient β_{ij} is the interaction between the ith and jth components of the beam. For $\beta_{ij} > 0$, the interaction is attractive; otherwise, the interaction is repulsive. Note that in the presence of strong periodic trapping potentials, the NLS Eqs. (2) can be approximated by the DNLS equations. For example, Eq. (3) describe a large class of discrete nonlinear systems such as optical fibers [11,12], small molecules such as benzene [13], and, more recently, dilute Bose-Einstein condensates trapped in a multiwell periodic potential [3,6,23,24].

The problem described in (2) has been considered in several cases. For $n = 1$, i.e. in one spatial dimension, the system (2) is integrable. Many analytical and numerical results on solitary wave solutions of m-component NLS equations are well-studied in, e.g. [10,14–16]. For $n = 2$ and $m = 1$, physical experiments in [21] 2-dimensional photorefractive screening solutions and a 2-dimensional self-trapped beam. It is natural to believe that there are 2-dimensional m-component ($m \geqslant 2$) solitons and self-trapped beams. A general theorem on the existence of high dimensional m-component solitons was first proved in [20]. In that paper, the authors show that the signs of the coupling coefficients β_{ij}'s are crucial for the existence of ground state solutions. For $m = 3$, when all the β_{ij}'s are positive, there exists a ground state solution, which is radially symmetric.

The motivations of this study are twofold. First, while the search of minimal energy solutions of the DNLS equations is of interest, non-linearity of the equations of the solutions prevents existing numerical schemes from being complete. In particular, while continuation and homotopy type schemes provide feasible ways for computing various solutions of the DNLS equations; it remains an challenge to assert the minimality of the computed solutions. Another motivation arises in a theoretical prediction reported recently. Lin and Wei [20] consider the case $V(\mathbf{z}) = 0$ and $m = 3$ with one repulsive and two attractive interactions. They show that if the coupling coefficients $|\beta_{ij}| \ll 1$ and the ground state solution exists, then the ground state cannot be radially symmetric. Computation of such non-radially symmetric energy minimizer can hardly be achieved by using continuation methods straightforwardly. The solution is actually "hidden" in the set of solutions and satiable routes leading to the target solution need to be identified.

In this article, we develop numerical schemes for computing minimal energy solutions of the m-component DNLS equations. The main contributions of this article are highlighted in the following items and the flowcharts in Fig. 1.

- We develop and prove a globally convergent fixed point iteration method (Fig. 1a) for computing the energy minimizers of the 1-component DNLS equation. In the case that the decoupled DNLS system has multiple minimizers, Algorithm 1 converges to a local minimizer that depends on the initial solution. However, if the decoupled DNLS system has a unique (and thus global) minimizer, which is true when $V(\mathbf{z}) = 0$ [19], Algorithm 1 is expected to converge to the global minimizer. These computed global energy minimizers are also used as the initial point of a continuation method for the 3-component DNLS equations with $V(\mathbf{z}) = 0$ to track other minimal energy solutions (Fig. 1c).
- We propose a scheme for tracking minimal energy solutions by a continuation method (Fig. 1b). To detect solution curves with minimal energy, we first show that the local minimal energy properties of the solutions remain unchanged between solution curve bifurcation points under mild assumptions. Consequently, whenever we detect a bifurcation point, we can probe each of the available bifurcation branches by checking the solution properties one step ahead to determine the target branch associated with the minimal energy solutions. By following this chosen branch, we can then track minimal energy solutions along a suitable solution curve.
- By integrating the above two schemes, we further develop a parameter-switching scheme (Fig. 1c) to qualitatively find the non-radially symmetric ground state in a 3-component DNLS equations system with two attractive interactions and one repulsive interaction and $V(\mathbf{z}) = 0$. The solution is predicted by [20] in an asymptotic setting. The proposed scheme confirms the existence of the solution numerically and visually.

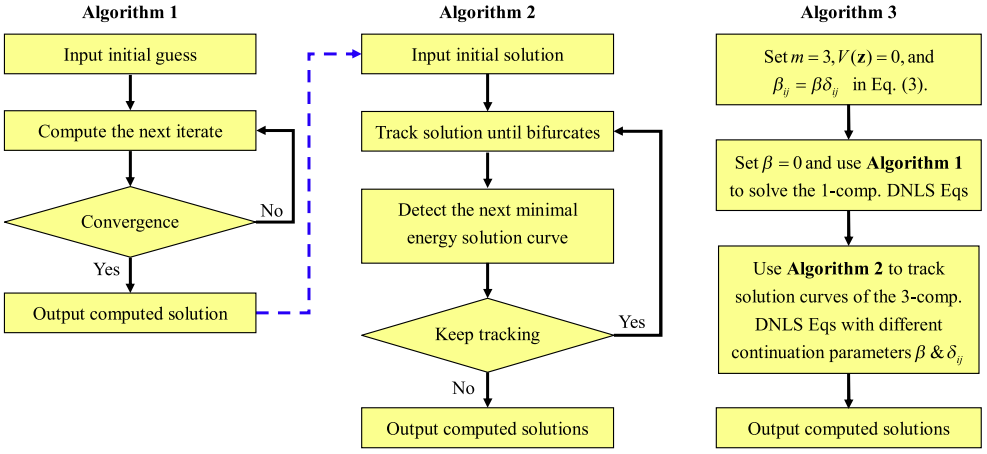

Fig. 1. Flowcharts of the algorithms proposed in this article. (a) Algorithm 1 (fixed point iteration) is used to find energy minimizers of the 1-component DNLS equation. (b) Algorithm 2 (minimal energy tracking continuation method) is used to track solution curves associated with minimal energy. (c) Algorithm 3 (continuation parameter switching method) is used to find the non-radially symmetric ground state predicted by [20].

It is worth noting that, in some other models, the DNLS equations is equipped with an extra normalization constraint on $\mathbf{u}_j$. The induced problem consequently becomes an eigenvalue problem. Numerical schemes such as [4,5,7–9] have been developed for solving such eigenvalue problems. However, they are not suitable for the target problem considered here.

To define the ground state solution to m-component cases, we first set the Nehari's manifold

$$\mathcal{N}_m = \Big\{ \boldsymbol{\phi} = (\phi_1, \ldots, \phi_m) \in (H^1(\Omega))^m \mid \ \phi_j \geqslant 0, \phi_j \not\equiv 0 \text{ and } \int_\Omega |\nabla \phi_j|^2 + \int_\Omega V(\mathbf{z})\phi_j^2 + \lambda_j \int_\Omega \phi_j^2 = \mu_j \int_\Omega \phi_j^4 + \sum_{i \neq j, i=1}^{m} \beta_{ij} \int_\Omega \phi_i^2 \phi_j^2, j = 1, \ldots, m \Big\},$$

and the energy functional

$$E(\boldsymbol{\phi}) = \sum_{j=1}^{m} \left(\frac{\int_\Omega |\nabla \phi_j|^2 + \int_\Omega V(\mathbf{z})\phi_j^2 + \lambda_j \int_\Omega \phi_j^2 - \frac{\mu_j}{2} \int_\Omega \phi_j^4}{2} + \right) - \frac{1}{4} \sum_{i,j=1, i \neq j}^{m} \beta_{ij} \int_\Omega \phi_i^2 \phi_j^2, \tag{4}$$

where $\boldsymbol{\phi} = (\phi_1, \ldots, \phi_m) \in (H^1(\Omega))^m$. Then, we consider the minimization problem

$$\inf_{\boldsymbol{\phi} \in \mathcal{N}_m} E(\boldsymbol{\phi}).$$

If $\boldsymbol{\phi} = (\phi_1, \ldots, \phi_m) \in \mathcal{N}_m$ has the following properties:

(i) $\phi_j > 0$ for all j and $\boldsymbol{\phi}$ satisfy (2);
(ii) $E(\boldsymbol{\phi}) \leqslant E(\boldsymbol{\psi})$ for any other solution $\boldsymbol{\psi}$ of (2),

then $\boldsymbol{\phi}$ is called a ground state solution of (2). In the case of $m = 1$ (1-component), the ground state solution of (2) can be obtained from the minimization problem

$$\inf_{\substack{\phi \geqslant 0 \\ \phi \in H^1(\Omega)}} \frac{\int_\Omega |\nabla \phi|^2 + \int_\Omega V(\mathbf{z})\phi^2 + \lambda \int_\Omega \phi^2}{\left(\int_\Omega \phi^4 \right)^{1/2}}, \tag{5}$$

up to a suitable normalization.

We define the corresponding energy functional for the m-component DNLS Eq. (3) as follows: the energy functional $E(\boldsymbol{\phi})$ in (4) becomes

$$E(\mathbf{u}) = \sum_{j=1}^{m} \left(\frac{-\mathbf{u}_j^\top \mathbf{A}\mathbf{u}_j + \lambda_j \mathbf{u}_j^\top \mathbf{u}_j - \frac{\mu_j}{2} \mathbf{u}_j^{②\top} \mathbf{u}_j^②}{2} \right) - \frac{1}{4} \sum_{i,j=1, i \neq j}^{m} \beta_{ij} \mathbf{u}_i^{②\top} \mathbf{u}_j^②, \tag{6}$$

where the vector $\mathbf{u} = (\mathbf{u}_1^\top, \ldots, \mathbf{u}_m^\top)^\top \in \mathbb{R}^{Nm}$ is in

$$\mathcal{N}_m = \left\{ (\mathbf{u}_1^\top, \ldots, \mathbf{u}_m^\top)^\top \in \mathbb{R}^{Nm} |\ \mathbf{u}_j \geqslant 0,\ \mathbf{u}_j \neq \mathbf{0} \text{ and } -\mathbf{u}_j^\top \mathbf{A}\mathbf{u}_j + \lambda_j \mathbf{u}_j^\top \mathbf{u}_j = \mu_j \mathbf{u}_j^{②\top} \mathbf{u}_j^② + \sum_{i \neq j, i=1}^{m} \beta_{ij} \mathbf{u}_i^{②\top} \mathbf{u}_j^②,\ \ j = 1, \ldots, m \right\}. \tag{7}$$

Throughout this paper, we use bold face letters or symbols to denote matrices or vectors. For $\mathbf{u} = (u_1, \ldots, u_N)^\top$, $[\![\mathbf{u}]\!] := \mathrm{diag}(\mathbf{u})$ denotes the diagonal matrix of $\mathbf{u}$ and $\|\mathbf{u}\|_4 = (\mathbf{u}^{②\top}\mathbf{u}^②)^{1/4}$. For $\mathbf{M} \in \mathbb{R}^{N\times N}, \mathbf{M} > 0 (\geqslant 0)$ denotes a positive (nonnegative) matrix with positive (nonnegative) entries, $\mathbf{M} \succ 0$ (with $\mathbf{M}^\top = \mathbf{M}$) denotes a symmetric positive definite matrix, and $\sigma(\mathbf{M})$ denotes the spectrum of $\mathbf{M}$.

This paper is organized as follows: in Section 2, we develop an iterative method to compute the positive ground state solution of 1-component DNLS equations and show that the iterative method is globally convergent. In Section 3, we discuss how we can track bifurcation branches in a continuation method to obtain local minimal energy solutions of the m-component DNLS equations. In Section 4, we propose a parameter-switching scheme to compute the non-radially symmetric ground state for the 3-component DNLS. Conclusion of the paper is given in Section 5.

2. Local and global energy minimizers of decoupled DNLS equations

We begin our discussion of numerical schemes and the corresponding analysis for solving 1-component DNLS equations. The solution of the decoupled equation is used as the initial solution of the m-component DNLS equations that $m > 1$. A fixed point iteration method is developed and analyzed for solving this 1-component DNLS equation. The computed solutions are local or global minimizers of the corresponding energy functional according to circumstances.

The 1-component DNLS equation is given by

$$\begin{cases} \mathbf{A}\mathbf{u} - \lambda\mathbf{u} + \mu\mathbf{u}^② \circ \mathbf{u} = \mathbf{0}, \\ \mathbf{u} > 0, \quad \mathbf{u} \in \mathbb{R}^N, \end{cases} \tag{8}$$

where λ and μ are positive constants. The variational problem corresponding to (5) can be formulated as

$$\inf_{\mathbf{u}\geqslant 0} \widehat{E}(\mathbf{u}), \tag{9a}$$

where

$$\widehat{E}(\mathbf{u}) = \frac{-\mathbf{u}^\top\mathbf{A}\mathbf{u} + \lambda\mathbf{u}^\top\mathbf{u}}{(\mathbf{u}^{②\top}\mathbf{u}^②)^{1/2}}. \tag{9b}$$

Formulation (9) is equivalent to minimize (6) subject to the constraint (7) with $m = 1$. Consequently, any solution $\mathbf{u} \in \mathbb{R}^N$ of (6) is a local minimum or a saddle point on the Nehari's manifold (7) with $m = 1$.

Next, we develop a fixed point iteration method for finding minimizers of (9) based on the following observations. The matrix $\mathbf{A}$ in (8) is generically diagonally dominant with nonnegative off-diagonal entries. That is, $-\mathbf{A}$ is an irreducible M-matrix. Let

$$\overline{\mathbf{A}} = \lambda\mathbf{I} - \mathbf{A}. \tag{10}$$

Then $\overline{\mathbf{A}}$ is an irreducible M-matrix because $\lambda > 0$. It follows that $\overline{\mathbf{A}}^{-1}$ is positive definite with positive entries (i.e. $\overline{\mathbf{A}}^{-1} \succ 0$ and $\overline{\mathbf{A}}^{-1} > 0$). We define the set

$$\mathcal{M} = \{\mathbf{u} \in \mathbb{R}^N |\ \|\mathbf{u}\|_4 = 1, \quad \mathbf{u} \geqslant 0\}, \tag{11}$$

It is easy to verify that if $\mathbf{u} \in \mathcal{M}$, then

$$\overline{\mathbf{A}}^{-1}\mathbf{u} = (\lambda\mathbf{I} - \mathbf{A})^{-1}\mathbf{u} > 0. \tag{12}$$

We now define a map $\mathbf{f} : \mathcal{M} \to \mathcal{M}$ by

$$\mathbf{f}(\mathbf{u}) = \frac{\overline{\mathbf{A}}^{-1}\mathbf{u}^③}{\|\overline{\mathbf{A}}^{-1}\mathbf{u}^③\|_4}. \tag{13}$$

Since the map $\mathbf{f}$ is well-defined by (12) and (13), we can use $\mathbf{f}$ to define the fixed point iteration $\mathbf{u}_{i+1} = \mathbf{f}(\mathbf{u}_i)$, as in the following algorithm.

Algorithm 1 (*Fixed point iteration*).

(i) Let $\overline{\mathbf{A}} \in \mathbb{R}^{N\times N}, \mathbf{u}_0 > 0$ with $\|\mathbf{u}_0\|_4 = 1$, and $i = 0$;

(ii) Solve the linear system

$$\overline{\mathbf{A}}\mathbf{u}_{i+1} = \mathbf{u}_i^③.$$

Compute $\mathbf{u}_{i+1} = \mathbf{u}_{i+1}/\|\mathbf{u}_{i+1}\|_4$.

(iii) If convergent, then $\mathbf{u}^* \leftarrow \mathbf{u}_{i+1}$, stop; else $i \leftarrow i + 1$, go to (ii).

Now, we analyze the convergence behavior of Algorithm 1. Detailed proofs of the theorems are given in Appendix A. First, we show that the 1-component DNLS Eq. (8) has a solution $\bar{\mathbf{u}}(\mu)$ and the solution can be computed by using the fixed point of $\mathbf{f}$.

Theorem 1. *The map $\mathbf{f}: \mathcal{M} \to \mathcal{M}$ given in (13) has a fixed point $\mathbf{u}^*$ in $\overset{\circ}{\mathcal{M}}$. Furthermore, the vector*

$$\bar{\mathbf{u}}(\mu) = \frac{1}{\mu^{1/2}} \|\overline{\mathbf{A}}^{-1}\mathbf{u}^{*③}\|_4^{-1/2}\mathbf{u}^* \in \mathcal{N}_1 \tag{14}$$

solves the 1-component DNLS Eq. (8).

Theorem 1 suggests solving the 1-component DNLS Eq. (8) by Algorithm 1. The following theorems further discuss how the solution sequence generated by Algorithm 1 converges to a fixed point of $\mathbf{f}$. In Theorem 2 below, we first show that the energy sequence corresponding to the iterates is decreasing, and therefore a subsequence of the iterates converges to a fixed point in $\mathcal{M}$ of $\mathbf{f}$. In Theorem 5 below, by making a mild assumption, we further show that the whole sequence $\{\mathbf{u}_i\}_{i=0}^{\infty}$ generated by Algorithm 1 converges to $\mathbf{u}^* \in \mathcal{M}$ globally.

Theorem 2. *(i) If $\mathbf{u} \in \mathcal{M}$ and $\mathbf{v} = \mathbf{f}(\mathbf{u})$, then $\widehat{E}(\mathbf{v}) \leqslant \widehat{E}(\mathbf{u})$, where $\widehat{E}(\cdot)$ is defined in (9b), and the equality holds if and only if $\mathbf{u}$ is a fixed point of $\mathbf{f}: \mathcal{M} \to \mathcal{M}$, i.e. $\mathbf{f}(\mathbf{u}) = \mathbf{u}$. (ii) For a sequence $\{\mathbf{u}_i\}_{i=0}^{\infty}$ generated by Algorithm 1, there exists a subsequence $\{\mathbf{u}_{n_i}\}_{i=0}^{\infty}$ such that*

$$\lim_{i\to\infty} \mathbf{u}_{n_i} = \mathbf{u}^*, \tag{15}$$

where $\mathbf{u}^* \in \mathcal{M}$ is a fixed point of the function $\mathbf{f}$ defined in (13).

The following corollary can be easily obtained by applying Theorem 2.

Corollary 3. *If the minimization problem (9) has a unique global minimizer $\mathbf{u}^* \in \mathcal{M}$, then there exists a neighborhood $R_{\mathbf{u}^*}$ of $\mathbf{u}^*$ such that the fixed point iteration converges to $\mathbf{u}^*$ for any initial vector $\mathbf{u}_0 \in R_{\mathbf{u}^*}$. In addition, $\bar{\mathbf{u}}(\mu)$, defined in (14), is a global minimizer of (9).*

Now, we discuss how the entire sequence generated by Algorithm 1 converges. To do so, we first define the $\overline{\mathbf{A}}$-norm of $\mathbf{u}$ by $\|\mathbf{u}\|_{\overline{\mathbf{A}}} = \sqrt{\mathbf{u}^\top \overline{\mathbf{A}}\mathbf{u}}$ and introduce the following lemma. Note that the definition of $\overline{\mathbf{A}}$-norm is well-defined, as $\overline{\mathbf{A}}$ is positive definite.

Lemma 4. *Let $\{\mathbf{u}_i\}_{i=0}^{\infty}$ be the sequence generated by Algorithm 1. We have*

$$\lim_{i\to\infty} \|\mathbf{u}_{i+1} - \mathbf{u}_i\|_{\overline{\mathbf{A}}} = 0. \tag{16}$$

Theorem 5 (Existence of a globally convergent sequence). *If $\mathbf{u}^*$ given in (15) is a strictly local minimum of (9), then the sequence $\{\mathbf{u}_i\}_{i=0}^{\infty}$ generated by Algorithm 1 converges to $\mathbf{u}^* \in \mathcal{M}$.*

In Theorem 5, we have shown that if a limit point $\mathbf{u}^*$ of $\{\mathbf{u}_i\}_{i=0}^{\infty}$ is a strictly local minimum of (9), then the sequence $\{\mathbf{u}_i\}_{i=0}^{\infty}$ generated by Algorithm 1 converges globally to $\mathbf{u}^* \in \overset{\circ}{\mathcal{M}}$ and $\mathbf{u}^*$ satisfies

$$(\lambda\mathbf{I} - \mathbf{A})\mathbf{u}^* = \tau\mathbf{u}^{*③} \text{ where } \tau = \|\overline{\mathbf{A}}^{-1}\mathbf{u}^{*③}\|_4.$$

We can then compute $\bar{\mathbf{u}}(\mu)$ by (14) to find the minimizers of the 1-component DNLS Eq. (8).

Remark 1. The 1-component NLS (i.e. Eq. (2) with $m = 1$) may associate with multiple local minimizers. In such cases, finding the global minimizer is a challenging task. However, in the case that $V(\mathbf{z}) = 0$, the 1-component NLS equation has a unique global minimizer [19]. Consequently, the computed solution $\bar{\mathbf{u}}(\mu)$ is expected to be the ground state solution of the 1-component DNLS Eq. (8), though in the absence of a rigorous proof. This computed ground state solution is then used in Section 4 as the initial of a continuation method for tracking the non-radially symmetric energy minimizer predicted in [20] that also assumes $V(\mathbf{z}) = 0$.

Remark 2. Algorithm 1 is similar to the continuous normalized gradient flow method (CNGFM) [5] in the sense that both methods generate energy decreasing sequences with mass conservation. Actually, Algorithm 1 can be formulated as a special case of CNGFM as shown below. However, a difference between the two methods does exist. The corresponding energy in each iteration of Algorithm 1 is decreased with step size equals 1 and the energy diminishing property holds for any initial vector $\mathbf{u}_0 \in \mathcal{M}$. In contrast, CNGFM does not guarantee the energy diminishing property, except the virtual time step Δt is sufficiently small. Such a requirement may slow down convergence rate in the scheme.

Now, we verify the claim given above. We first note that we consider problem (9) for the 1-component DNLS equations. Since $\widehat{E}(\mathbf{u}) = \widehat{E}(c\mathbf{u})$ for $c > 0$, it is natural to find the minimizers on a "unit sphere". Here, we choose $\mathcal{M}$, which is defined in (11), as the restriction set. Problem (9) is thus transformed to be the form:

$$\min_{\mathbf{u}\in\mathcal{M}} \mathbf{u}^\top \overline{\mathbf{A}}\mathbf{u}, \tag{17}$$

where $\overline{\mathbf{A}} = \lambda I - \mathbf{A}$. Let $\widetilde{E}(\mathbf{u}) = \frac{1}{2}\mathbf{u}^\top \overline{\mathbf{A}}\mathbf{u} - \frac{1}{2}\sqrt{\mathbf{u}^{②\top}\mathbf{u}^{②}}$ and consider the minimization problem

$$\min_{\mathbf{u}\in\mathcal{M}} \widetilde{E}(\mathbf{u}). \tag{18}$$

One can easily verify that the problems (9), (17) and (18) have the same minimizer. In the following, we shall focus on problem (18). Taking gradient of $\widetilde{E}(\mathbf{u})$, we have

$$\nabla\widetilde{E}(\mathbf{u}) = \overline{\mathbf{A}}\mathbf{u} - (\mathbf{u}^{②\top}\mathbf{u}^{②})^{-1/2}\mathbf{u}^{③}.$$

By applying the CNGFM, we have

$$\begin{cases} \mathbf{u}_t(t) = -\nabla\widetilde{E}(\mathbf{u}(t)), \quad t_n < t < t_{n+1} = t_n + \Delta t,\ n > 0, \\ \mathbf{u}(t_{n+1}) := \mathbf{u}(t_{n+1}^+) = \mathbf{u}(t_{n+1}^-)/\|\mathbf{u}(t_{n+1}^-)\|_4. \end{cases} \tag{19}$$

By further discretizing (19), we have the following semi-implicit time discretization scheme

$$\begin{cases} \frac{\tilde{\mathbf{u}}_{n+1}-\mathbf{u}_n}{\Delta t} = -(\overline{\mathbf{A}} - I)\tilde{\mathbf{u}}_{n+1} - \mathbf{u}_n + (\mathbf{u}_n^{②\top}\mathbf{u}_n^{②})^{-1/2}\mathbf{u}_n^{③}, \\ \mathbf{u}_{n+1} := \tilde{\mathbf{u}}_{n+1}/\|\tilde{\mathbf{u}}_{n+1}\|_4. \end{cases} \tag{20}$$

Taking $\Delta t = 1$ and using the fact that $\|\mathbf{u}_n\|_4 = 1$, (20) can be reduced to

$$\begin{cases} \tilde{\mathbf{u}}_{n+1} = \overline{\mathbf{A}}^{-1}\mathbf{u}_n^{③}, \\ \mathbf{u}_{n+1} := \tilde{\mathbf{u}}_{n+1}/\|\tilde{\mathbf{u}}_{n+1}\|_4. \end{cases}$$

This is exactly the fixed point iteration (Algorithm 1) proposed in this section for solving minimizers of the 1-component DNLS equations. Consequently, we claim that the fixed point iteration is a special case of the CNGFM with a large time step $\Delta t = 1$.

3. The minimal energy tracking continuation method

Now, we focus on how to track minimal energy solutions in the framework of continuation methods. After a brief introduction of continuation methods, we discuss the technique for tracking minimal energy solutions. At the end of this section, we integrate all the proposed ideas into a continuation method algorithm for tracking minimal energy solutions.

3.1. General framework of continuation methods

We briefly introduce a general framework of a continuation method for the m-component DNLS Eq. (3). For a detailed discussion of the continuation scheme, see [2,8,17,18], for example.

Denote the continuation parameter by $\beta \geqslant 0$, and rewrite the m-component DNLS Eq. (3) as

$$\mathbf{G}(\mathbf{x}, \beta) = \mathbf{0}, \tag{21}$$

where $\mathbf{x} = (\mathbf{u}_1^\top, \ldots, \mathbf{u}_m^\top)^\top \in \mathbb{R}^{mN}$ and $\mathbf{G} = (\mathbf{G}_1, \ldots, \mathbf{G}_m) : \mathbb{R}^{mN} \times \mathbb{R} \to \mathbb{R}^{mN}$ is a smooth mapping with

$$\mathbf{G}_j(\mathbf{x}, \beta) = \mathbf{A}\mathbf{u}_j - \lambda_j(\beta)\mathbf{u}_j + \mu_j(\beta)\mathbf{u}_j^{②} \circ \mathbf{u}_j + \sum_{i\neq j, i=1}^{m} \beta_{ij}(\beta)\mathbf{u}_i^{②} \circ \mathbf{u}_j, \tag{22}$$

for $j = 1, \ldots, m$. The parameters λ_j, μ_j, and β_{ij} in (22) may depend on β. One example is to fix λ_j and μ_j and set $\beta_{ij}(\beta) = \beta\beta_{ij}$. Furthermore, we define the solution curve of (21) as

$$\mathcal{C} = \{\mathbf{y}(s) = (\mathbf{x}(s)^\top, \beta(s))^\top \mid \mathbf{G}(\mathbf{y}(s)) = \mathbf{0},\ s \in \mathbb{R}\}, \tag{23}$$

assuming that a parametrization via arc-length s is available.

Two main components of a continuation method are to follow the solution curve and to test bifurcation points. To follow the solution curve, we use the prediction-correction process. Suppose $\mathbf{y}_i(s) = (\mathbf{x}_i^\top(s), \beta_i(s))^\top \in \mathbb{R}^{mN+1}$ is a solution lying (approximately) on the solution curve $\mathcal{C}$. Starting from the point $\mathbf{y}_i(s)$, standard continuation methods usually take the tangent vector of the solution curve at $\mathbf{y}_i(s)$ as the prediction vector. In particular, the tangent vector can be computed by solving the linear system

$$\mathcal{D}\mathbf{G}(\mathbf{y}(s))\dot{\mathbf{y}}(s) = \mathbf{0},$$

which is obtained by differentiating Eq. (21) with respect to s. Here $\dot{\mathbf{y}}(s) = (\dot{\mathbf{x}}(s)^\top, \dot{\beta}(s))^\top$ is a tangent vector of $\mathcal{C}$ at $\mathbf{y}(s)$, and

$$\mathcal{D}\mathbf{G}(\mathbf{y}(s)) = [\mathbf{G}_{\mathbf{x}}(\mathbf{y}(s)), \mathbf{G}_\beta(\mathbf{y}(s))] \in \mathbb{R}^{mN\times(mN+1)} \tag{24}$$

denotes the Jacobian matrix of $\mathbf{G}$ at $\mathbf{y}(s)$. To track the solution curve described in (23), we first find the Euler predictor

$$\mathbf{y}_{i+1,1} = \mathbf{y}_i + h_i\dot{\mathbf{y}}_i, \tag{25}$$

where $h_i > 0$ is the step length and $\dot{\mathbf{y}}_i$ is the normalized tangent vector at $\mathbf{y}_i$. Newton's method is then used to find the corrector to improve the accuracy of $\mathbf{y}_{i+1,1}$. More precisely, for the correction vector $\boldsymbol{\delta}_l$, the iteration

$$\mathbf{y}_{i+1,l+1} = \mathbf{y}_{i+1,l} + \boldsymbol{\delta}_l \tag{26}$$

is computed for $l = 1, 2, \ldots$ until a convergence criterion is satisfied for $l = l_\infty$ and we take

$$\mathbf{y}_{i+1} = \mathbf{y}_{i+1,l_\infty} \tag{27}$$

as a new approximate solution on the solution curve $\mathcal{C}$.

To test bifurcations, we rely on Theorem 6. The theorem gives conditions under which a point on the solution curve is a bifurcation point. The theoretical and numerical details for detecting bifurcation points of the solution curve $\mathcal{C}$ and for tracing the bifurcation branches can be found in [8,18].

Note that from Theorem 6, we see that a bifurcation point occurs when the matrix $\mathbf{G}_\mathbf{x}$ is singular.

Theorem 6 (Bifurcation Test [17]). *Let $\mathcal{C}$ in (23) be a smooth curve of (21) parameterized by s. Suppose* $\det(\mathbf{G}_\mathbf{x}(\mathbf{y}(s)))$ *changes sign at s^*. Then $\mathbf{y}(s^*)$ is a bifurcation point of (21).*

We have discussed how we follow the solution curve and detect bifurcation points in the continuation method. In the next sub-section, we focus on how we may determine the bifurcation branches associated with minimal energy solutions.

3.2. Minimal energy tracking

In this sub-section, we discuss how to determine whether a solution to the DNLS Eq. (3) is a local minimum of $E(\mathbf{x})$ on Nehari's manifold $\mathcal{N}_m$. The main result is that each bifurcation point of the solution curve $\mathcal{C}$ coincides with a bifurcation of critical points for $E(\mathbf{x})$ on $\mathcal{N}_m$, as will be shown in Theorem 10.

First, we define the necessary notation and discuss how to verify local minimum of $E(\mathbf{x})$ on $\mathcal{N}_m$ by applying standard optimization techniques to the optimization problem

$$\inf_{\mathbf{x}\in\mathcal{N}_m} E(\mathbf{x}), \tag{28}$$

where the energy functional $E(\mathbf{x})$ and Nehari's manifold $\mathcal{N}_m$ are defined by (6) and (7), respectively. We define the Lagrangian function of the optimization problem (28) as

$$\mathcal{L}(\mathbf{x}, \boldsymbol{v}) = E(\mathbf{x}) - \sum_{j=1}^{m} v_j g_j(\mathbf{x}), \tag{29}$$

where $g_j(\mathbf{x}) = \mathbf{u}_j^\top \mathbf{A}\mathbf{u}_j - \lambda_j \mathbf{u}_j^\top \mathbf{u}_j + \mu_j \mathbf{u}_j^{②\top} \mathbf{u}_j^② + \sum_{i\neq j, i=1}^m \beta_{ij} \mathbf{u}_i^{②\top} \mathbf{u}_j^②$, and $\boldsymbol{v} = (v_1, \ldots, v_m)^\top \in \mathbb{R}^m$ are the Lagrange multipliers. Furthermore, the discretized Nehari's manifold $\mathcal{N}_m$ defined in (7) can be written as

$$\mathcal{N}_m = \{(\mathbf{u}_1^\top, \ldots, \mathbf{u}_m^\top)^\top \in \mathbb{R}^{mN} | \mathbf{u}_j \geqslant 0, \quad \mathbf{u}_j \neq 0 \text{ and } g_j(\mathbf{x}) = 0,\ j = 1, \ldots, m\}.$$

The total derivative of the function $\mathbf{g} = (g_1, \ldots, g_m)^\top$

$$\nabla \mathbf{g}(\mathbf{x}) = \begin{bmatrix} \nabla g_1(\mathbf{x}) \\ \vdots \\ \nabla g_m(\mathbf{x}) \end{bmatrix} \in \mathbb{R}^{m\times mN}, \tag{30}$$

where $\nabla g_j(\mathbf{x})$ is the row vector given by

$$(\nabla g_j(\mathbf{x}))_i = \begin{cases} 2\beta_{ij} \mathbf{u}_i \circ \mathbf{u}_j^②, & i \neq j, \\ 2(\mathbf{A}\mathbf{u}_j - \lambda_j \mathbf{u}_j + 2\mu_j \mathbf{u}_j^② \circ \mathbf{u}_j + \sum\limits_{i\neq j, i=1}^{m} \beta_{ij} \mathbf{u}_i^② \circ \mathbf{u}_j), & i = j. \end{cases} \tag{31}$$

The following theorem gives a test to determine whether a point $\mathbf{x} \in \mathbb{R}^{mN}$ is a local minimum of $E(\mathbf{x})$ on $\mathcal{N}_m$ or not.

Theorem 7 (Nocedal–Wright [22]). *Let $\mathbf{x}$ be a point in $\mathbb{R}^{mN}$. Suppose that the Karush–Kuhn–Tucker (KKT) conditions*

$$\nabla_\mathbf{x} \mathcal{L}(\mathbf{x}, \boldsymbol{v}) = \mathbf{0} \text{ and } \mathbf{x} \in \mathcal{N}_m \tag{32}$$

are satisfied for a certain $\boldsymbol{v} \in \mathbb{R}^m$. Suppose also that

$$\mathbf{w}^\top \nabla^2_{\mathbf{x}\mathbf{x}} \mathcal{L}(\mathbf{x}, \boldsymbol{v}) \mathbf{w} > 0, \quad \text{for all } \mathbf{w} \in C(\mathbf{x}, \boldsymbol{v}),\ \mathbf{w} \neq \mathbf{0}, \tag{33}$$

where $C(\mathbf{x}, \boldsymbol{v})$ is the null space of $\nabla \mathbf{g}(\mathbf{x})$ in (30). Then $\mathbf{x}$ is a strict local minimum solution of $E(\mathbf{x})$ on $\mathcal{N}_m$.

Furthermore, we derive the relations between the DNLS Eq. (21) and the optimization problem (28) in the following remarks.

1. All solution points lying on the solution curve $\mathcal{C}$ of DNLS equation satisfy the KKT conditions (32) with $\boldsymbol{\nu} = \mathbf{0}$. From (29) and Theorem 7, a point $\mathbf{x}$ that satisfies the KKT conditions is the solution of

$$\nabla_{\mathbf{x}} E(\mathbf{x})^{\top} - \nabla \mathbf{g}(\mathbf{x})^{\top} \boldsymbol{\nu} = \mathbf{0} \text{ and } \mathbf{x} \in \mathcal{N}_m,$$

where $\nabla \mathbf{g}(\mathbf{x})$ is given in (30) and $\nabla_{\mathbf{x}} E(\mathbf{x}) = (\nabla_{\mathbf{u}_1} E(\mathbf{x}), \ldots, \nabla_{\mathbf{u}_m} E(\mathbf{x})) \in \mathrm{R}^{mN}$ with

$$\nabla_{\mathbf{u}_j} E(\mathbf{x})^{\top} = \mathbf{A}\mathbf{u}_j - \lambda_j \mathbf{u}_j + \mu_j \mathbf{u}_j^{②} \circ \mathbf{u}_j + \sum_{i \neq j, i=1}^{m} \beta_{ij} \mathbf{u}_i^{②} \circ \mathbf{u}_j.$$

Since the equation $\nabla_{\mathbf{x}} E(\mathbf{x}) = \mathbf{0}$ is actually the DNLS Eq. (21), we see that if $\mathbf{y} = (\mathbf{x}^{\top}, \beta)^{\top}$ is a solution of the DNLS Eq. (21), then $\mathbf{x} \in \mathcal{N}_m$ and $\nabla_{\mathbf{x}} \mathcal{L}(\mathbf{x}, \mathbf{0}) = \mathbf{0}$. That is, all points on the solution curve $\mathcal{C}$ of the DNLS equation satisfy the KKT conditions (32) with $\boldsymbol{\nu} = \mathbf{0}$.

2. We define the projected Hessian matrix $\mathbf{H}(\mathbf{y}(s^*))$, to be used later for testing positive definiteness. Let $\mathbf{y} = (\mathbf{x}^{\top}, \beta)^{\top}$ be a point on $\mathcal{C}$. We define the projected Hessian matrix at $\mathbf{y}$ to be

$$\mathbf{H}(\mathbf{y}) \equiv \mathbf{P}(\mathbf{x})^{\top} \nabla^2_{\mathbf{xx}} \mathcal{L}(\mathbf{x}, \mathbf{0}) \mathbf{P}(\mathbf{x}) = \mathbf{P}(\mathbf{x})^{\top} \mathbf{G}_{\mathbf{x}}(\mathbf{y}) \mathbf{P}(\mathbf{x}), \tag{34}$$

where $\mathbf{G}_{\mathbf{x}}(\mathbf{y})$ is given in (24). Here $\mathbf{P}(\mathbf{x}) \in \mathbb{R}^{mN \times \ell}$ is the matrix whose columns form an orthonormal basis of the null space of $\nabla \mathbf{g}(\mathbf{x})$. In other words,

$$[\nabla \mathbf{g}(\mathbf{x})] \mathbf{P}(\mathbf{x}) = \mathbf{0}, \tag{35}$$

and if $\nabla \mathbf{g}(\mathbf{x})$ is of full row rank, then $\ell = mN - m$.

3. Applying the above two remarks and considering the path $\mathbf{y}(s)$ that describes the solution curve $\mathcal{C}$, observe that if $\mathbf{y}(s)$ is a local minimum of (28) for $s < s^*$ and a saddle point for $s > s^*$, then from (33) in Theorem 7, the projected Hessian matrix $\mathbf{H}(\mathbf{y}(s^*))$ is singular.

We have presented the relations between the DNLS Eq. (21) and the optimization problem (28). Now, we develop the relations between the solution curve bifurcation and the critical point bifurcation by applying Theorem 6 (for the solution curve bifurcation test) and Theorem 7 (for the optimality test). Specifically, in Lemma 8, we show that for each bifurcation point $\mathbf{y}^* = \mathbf{y}(s^*) \in \mathcal{C}$, i.e. where the matrix $\mathbf{G}_{\mathbf{x}}(\mathbf{y}^*)$ is singular, the projected Hessian matrix $\mathbf{H}(\mathbf{y}^*)$ is singular. In Lemma 9, we show that the converse of Lemma 8 is true whenever the auxiliary matrix $\boldsymbol{\Sigma}(\mathbf{y})$ is invertible. Here

$$\boldsymbol{\Sigma}(\mathbf{y}) = (2\beta_{ij} \mathbf{u}_i^{②\top} \mathbf{u}_j^{②}), \tag{36}$$

and we set $\beta_{ii} = \mu_i$.

Lemma 8. *Let $\mathbf{y}^*$ be a bifurcation point of the DNLS* Eq. (21) *along the solution curve $\mathcal{C}$. Then* $\det(\mathbf{H}(\mathbf{y}^*)) = 0$.

Lemma 9. *Let $\mathbf{y}^* \in \mathcal{C}$. If* $\det(\mathbf{H}(\mathbf{y}^*)) = 0$ *and $\boldsymbol{\Sigma}(\mathbf{y}^*)$ is invertible, then* $\det(\mathbf{G}_{\mathbf{x}}(\mathbf{y}^*)) = 0$.

The above two lemmas suggest the following result. Let $\mathbf{y}^* \in \mathcal{C}$ and $\boldsymbol{\Sigma}(\mathbf{y}^*)$ be an invertible matrix, then $\det(\mathbf{H}(\mathbf{y}^*)) = 0$ if and only if $\det(\mathbf{G}_{\mathbf{x}}(\mathbf{y}^*)) = 0$. In other words, the bifurcation of the solution curves $\mathcal{C}$ and the bifurcation of the critical points for $E(\mathbf{x})$ on $\mathcal{N}_m$ occur at exactly the same points.

Combining Lemmas 8 and 9, we can see that solutions lying on a so-called "solution segment" have the same critical point characteristics. Before giving the rigorous statement of the result in Theorem 10, we first define the solution segment. Let $\mathbf{y}_0 = \mathbf{y}(s_0)$ be any regular point (i.e. $\det(\mathbf{G}_{\mathbf{x}}(\mathbf{y}_0)) \neq 0$) of the solution curve $\mathcal{C}$. Let $\Gamma_{seg}(\mathbf{y}_0) \subseteq \mathcal{C}$ be a maximal connected set without bifurcation point and containing y_0. That is, a solution segment

$$\Gamma_{seg}(\mathbf{y}_0) = \{\mathbf{y}(s) \in \mathcal{C} \mid \det(\mathbf{G}_{\mathbf{x}}(\mathbf{y}(\bar{s}))) \neq 0 \text{ for } \bar{s} \text{ between } s_0 \text{ and } s\}. \tag{37}$$

Now, we state the theorem that can be used to choose suitable bifurcation branches that lead to minimal energy solutions while bifurcations occur.

Theorem 10. *Let $\mathbf{y}_0 = (\mathbf{x}_0^{\top}, \beta_0)^{\top} \in \mathcal{C}$ with* $\det(\mathbf{G}_{\mathbf{x}}(\mathbf{y}_0)) \neq 0$ *and suppose that $\boldsymbol{\Sigma}(\mathbf{y})$ is invertible for each $\mathbf{y} \in \Gamma_{seg}(\mathbf{y}_0)$. If $\mathbf{x}_0$ is a strict local minimum solution of $E(\mathbf{x})$ on $\mathcal{N}_m$, then for each $\mathbf{y} = (\mathbf{x}^{\top}, \beta)^{\top} \in \Gamma_{seg}(\mathbf{y}_0)$, $\mathbf{x}$ is a strict local minimum solution of $E(\mathbf{x})$ on $\mathcal{N}_m$.*

In summary, Theorem 10 suggests that along the solution curve $\mathcal{C}$ tracked by a continuation method, if the initial point is a local minimum of $E(\mathbf{x})$ on $\mathcal{N}_m$ and the local minimum becomes a saddle point somewhere along the solution curve, then it must meet a bifurcation point under some mild assumptions. Consequently, whenever we detect a bifurcation point, we can track each of the available bifurcation branches one step ahead and test the positivity of the corresponding projected Hessian matrices. According to Theorem 10, we can then determine which one is the local minimum energy branch.

3.3. The overall algorithm

Finally, we conclude this section by proposing the minimal energy tracking continuation method (METCM) in Algorithm 2.

Algorithm 2 (*Minimal energy tracking continuation method (METCM)*).

(i) [Initialization] Determine an initial solution $\mathbf{y}(0)$ by letting $\beta(0) = 0$ (e.g. use Algorithm 1 to solve the resulting decoupled DNLS equations).
(ii) [Solution curve following] Iterate until bifurcation occurs.
  (a) Compute the next solution $\mathbf{y}(s)$ by the predictor–corrector scheme described in (25)–(27).
  (b) Detect the bifurcation point by Theorem 6 and techniques described in [8,18].
(iii) [Minimal energy solution curve detection]
  (a) Track one step ahead for each of the available bifurcation branches.
  (b) Test the positiveness of the corresponding projected Hessian matrices.
  (c) Pick one bifurcation branch with positive projected Hessian matrices as the next minimal energy solution curve to be followed.
(iv) Go to Step (ii) to follow the next solution curve or stop.

Note that in Step (i) of the algorithm, we may set $\beta_{ij} = 0$ and solve the decoupled DNLS Eq. (3) by Algorithm 1 and (14) to obtain the initial solution $\mathbf{y}(0) = ((\bar{\mathbf{u}}, \bar{\mathbf{u}}, \bar{\mathbf{u}})^\top, 0)^\top$ for $m = 3$. In Step (iii-b), it is possible to identify more than one minimal energy branch. We can track all these branches simultaneously in parallel computations.

To conclude this section, we give a simple example to illustrate the key components discussed in this section. The main goal is to show how we can track energy minimizers of $E(x) = 0.5x^4 + (1-\beta)x^2$ by the METCM. Here, $x \in \mathbb{R}$ and β is the continuation parameter. By setting $G(x,\beta) := E'(x) = 2x^2 + 2(1-\beta)x$, we can see that (i) the solutions of $G(x,\beta) = 0$ are actually the critical points of $E(x)$, (ii) the solution curve $\mathcal{C}$ of $G(x,\beta) = 0$ is the union of the trivial curve $\mathcal{C}_0 = \{(0,\beta)|\ \beta \in \mathbb{R}\}$ and the parabolic curve $\mathcal{C}_p = \{(\pm\sqrt{\beta-1}, \beta)|\ \beta > 1\}$, (iii) $y^* = (0,1) \in \mathcal{C}_0$ is a bifurcation point, as $\mathcal{C}_0$ is a smooth curve with parameter β and $G_x(0,\beta) = 2(1-\beta)$ changes sign at $\beta^* = 1$.

Theorem 6, and (iv) The local minima of $E(x)$ occur at 0 for $\beta < 1$ and at $\pm\sqrt{\beta-1}$ for $\beta > 1$.

Starting from $y_0 = (0,0) \in \mathcal{C}$, we track the solution curve until we meet the bifurcation point $y^* = (0,1)$. As the point $y_0 = (0,0)$ is a strict local minimum of $E(x)$ with $\det(G_x(y_0)) \neq 0$ and $\det(G_x(y^*)) = 0$, Theorem 10 suggests that all the solutions on the solution segment, as defined in (37), $\Gamma_{seg}(y_0) = \{(0,\beta)|\ \beta < 1\}$ are all strict local minimizers. To detect minimal energy solution curve as suggested in Step (iii) of Algorithm 2, we take one step ahead on the three available bifurcation branches and test the points $\left(\sqrt{\beta-1}, \beta\right), \left(-\sqrt{\beta-1}, \beta\right)$ and $(0,\beta)$ for $\beta = 1^+$ to determine the next minimal energy curve to be followed. By doing so, we can track the local minimum energy curve $\mathcal{C}_p$ rather than $\{(0,\beta)|\ \beta > 1\}$. It is worth noting that, a straightforward calculation can verify that the local minimum curve of $E(x)$ is $\Gamma_{seg}(y_0) \cup \mathcal{C}_p$, which matches the results obtained by the METCM exactly.

4. Minimal energy tracking for non-radially symmetric solutions

In this section, we demonstrate the capabilities of the METCM by finding non-trivial minimal energy solutions of a 3-component DNLS problem that has one repulsive and two attractive interactions and assumes $V(\mathbf{z}) = 0$. Our main tools are threefold: the computation of the ground states of the decoupled DNLS equations in Section 2, the minimal energy tracking continuation method in Section 3, and a parameter-switching scheme to be discussed below. By combining these techniques, we can find a 3-component non-radially symmetric energy minimizer while β_{ij} approaches zero. The existence of such non-radially symmetric solution has been predicted by Lin and Wei theoretically [20] for $m = 3$ and $V(\mathbf{z}) = 0$ in Eqs. (2). They show that with one repulsive and two attractive interactions, if the coupling coefficients $|\beta_{ij}| \ll 1$, and the ground state solution exists, then the ground state must be non-radially symmetric. Furthermore, the corresponding energy is smaller than the energy of the positive radially symmetric solution.

Using notations similar to those in [20], we consider the following 3-component DNLS equations by assuming $\lambda_1 = \lambda_2 = \lambda_3 = \mu_1 = \mu_2 = \mu_3 = 1$. We also rewrite $\beta_{ij} = \beta\delta_{ij}$ and assume $\delta_{12} = \delta_{21}, \delta_{13} = \delta_{31}$, and $\delta_{23} = \delta_{32}$,

$$\mathbf{A}\mathbf{u}_1 - \mathbf{u}_1 + \mathbf{u}_1^{③} + \beta\delta_{21}\mathbf{u}_2^{②}\mathbf{u}_1 + \beta\delta_{31}\mathbf{u}_3^{②}\mathbf{u}_1 = \mathbf{0}, \tag{38a}$$

$$\mathbf{A}\mathbf{u}_2 - \mathbf{u}_2 + \mathbf{u}_2^{③} + \beta\delta_{12}\mathbf{u}_1^{②}\mathbf{u}_2 + \beta\delta_{32}\mathbf{u}_3^{②}\mathbf{u}_2 = \mathbf{0}, \tag{38b}$$

$$\mathbf{A}\mathbf{u}_3 - \mathbf{u}_3 + \mathbf{u}_3^{③} + \beta\delta_{13}\mathbf{u}_1^{②}\mathbf{u}_3 + \beta\delta_{23}\mathbf{u}_2^{②}\mathbf{u}_3 = \mathbf{0}. \tag{38c}$$

Note that the matrix $\mathbf{A}$ in Eqs. (38) is the discretization matrix of the Laplacian only as $V(\mathbf{z}) = 0$.

To the best of our knowledge, such non-radially symmetric solutions have not been computed and visualized numerically. Simple straightforward numerical methods cannot lead to non-radially symmetric solutions. For example, only radially symmetric solutions are found for small β_{ij}'s if we simply follow the solution curve

$$\mathcal{C}_\beta = \{(\mathbf{x}^\top, \beta)^\top|\ \mathbf{G}(\mathbf{x},\beta) = \mathbf{0} \text{ is given in (38) with } \delta_{12} = \delta_{13} = 1 \text{ and } \delta_{23} = -1, \text{for } \beta \in \mathbb{R}_+\}.$$

by starting from $\beta = 0$ [18].

Now, we describe how we can find the non-radially symmetric solutions for the case of one repulsive and two attractive interactions in the 3-component DNLS Eqs. (38). We first propose a continuation parameter-switching scheme with an auxiliary illustration in Fig. 2. Then we describe the motivations behind the scheme.

Algorithm 3 (*Continuation parameter switching method*).

(i) Compute the initial solution $(\bar{\mathbf{u}}, \bar{\mathbf{u}}, \bar{\mathbf{u}})$ by Algorithm 1, where $\bar{\mathbf{u}}$ is the solution of the 1-component DNLS (or the decoupled DNLS for $\beta = 0$).

(ii) Let β be the continuation parameter. Use METCM to track the solution curve

$$\mathcal{C}_1 = \{(\mathbf{x}^\top, \beta)^\top \mid \mathbf{G}(\mathbf{x}, \beta) = \mathbf{0} \text{ is given in}(38) \text{ with } \delta_{12} = \delta_{13} = \delta_{23} = 1, \text{ for } 0 \leqslant \beta \leqslant 0.2\}$$

from $\beta = 0$ to $\beta = 0.2$.

(iii) Let δ_{23} be the continuation parameter and fix $\beta = 0.2$. Use METCM to track the solution curve

$$\mathcal{C}_2 = \{(\mathbf{x}^\top, \delta_{23})^\top \mid \mathbf{G}(\mathbf{x}, \delta_{23}) = \mathbf{0} \text{ is given in}(38) \text{ with } \beta = 0.2, \ \delta_{12} = \delta_{13} = 1, \text{ for } -1 \leqslant \delta_{23} \leqslant 1\}.$$

from $\delta_{23} = 1$ to $\delta_{23} = -1$.

(iv) Let β be the continuation parameter. Use METCM to track the solution curve

$$\mathcal{C}_3 = \{(\mathbf{x}^\top, \beta)^\top \mid \mathbf{G}(\mathbf{x}, \beta) = \mathbf{0} \text{ is given in}(38) \text{ with } \delta_{12} = \delta_{13} = 1 \text{ and } \delta_{23} = -1, \text{ for } \beta \in \mathbb{R}\},$$

from $\beta = 0.2$ to $\beta \approx 0_+$.

We implement Algorithm 3 on a square domain $[-5, 5] \times [-5, 5]$ with grid size $h = 0.2$. We plot the conceptual solution curves (with bifurcation points) and the corresponding energy curves of $\mathcal{C}_2$ in Figs. 3 and 4, respectively. We use the same curve styles in these two figures to indicate the corresponding solution curves. Similarly, the bifurcation diagram and energy curves of $\mathcal{C}_3$ are shown in Figs. 5 and 6, respectively. In the solution curves (i.e. Figs. 3 and 5) the corresponding nodal domains of three positive bound state solutions of certain segments of the solution curves are attached in triples near the solution curves. In each of the nodal domain triples, the left, middle and right figures are the density plots of $\mathbf{u}_1, \mathbf{u}_2$ and $\mathbf{u}_3$,

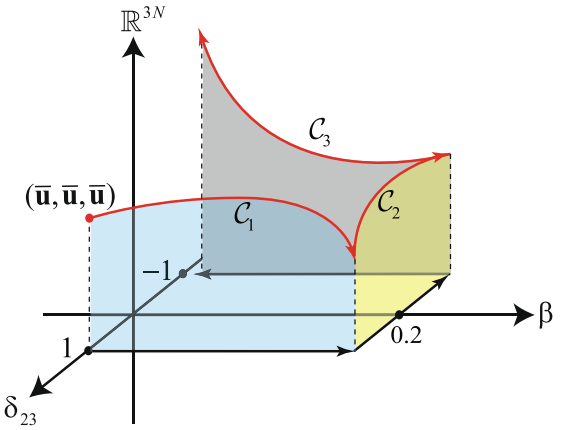

Fig. 2. Illustration for the curves $\mathcal{C}_1, \mathcal{C}_2$ and $\mathcal{C}_3$ in Steps (ii)–(iv) of Algorithm 3.

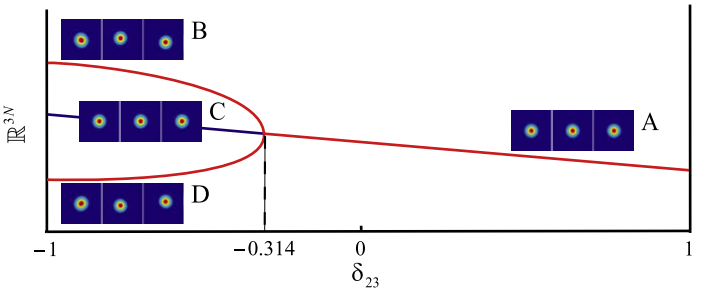

Fig. 3. A bifurcation diagram of the solution curve for $\mathcal{C}_2 = \{(\mathbf{x}^\top, \delta_{23})^\top \mid \mathbf{G}(\mathbf{x}, \delta_{23}) = \mathbf{0}$ is given in (38) with $\beta = 0.2, \delta_{12} = \delta_{13} = 1$, for $-1 \leqslant \delta_{23} \leqslant 1\}$.

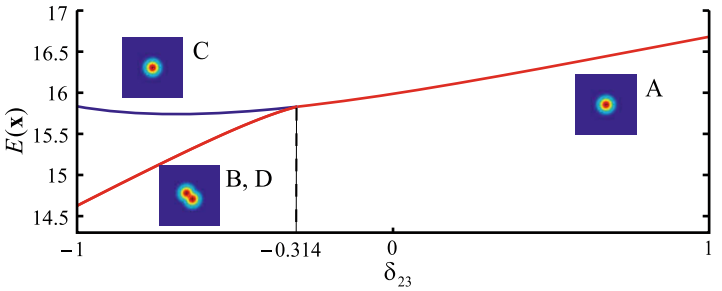

Fig. 4. Energy curve of $\mathcal{C}_2$.

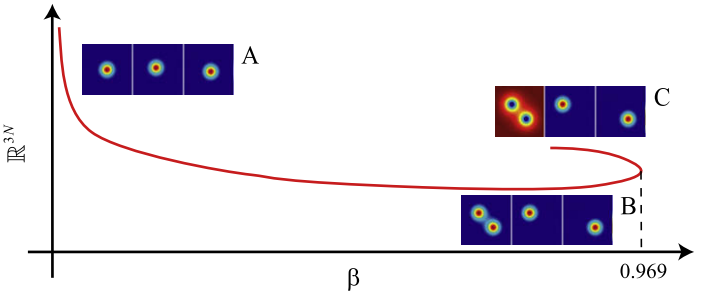

Fig. 5. A bifurcation diagram of the solution curve for $\mathcal{C}_3 = \{(\mathbf{x}^\top, \beta)^\top \mid \mathbf{G}(\mathbf{x}, \beta) = \mathbf{0}$ is given in (38) with $\delta_{12} = \delta_{13} = 1$ and $\delta_{23} = -1$, for $\beta \in \mathbb{R}\}$.

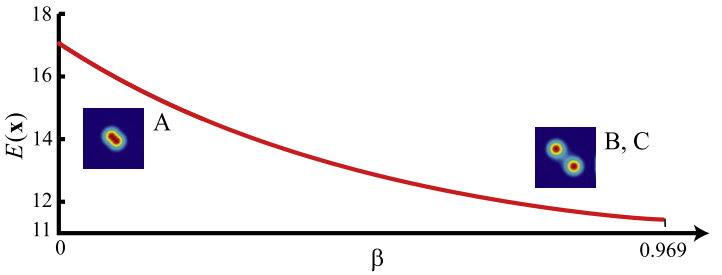

Fig. 6. Energy curve of $\mathcal{C}_3$.

respectively. As the solution formats remain similar unless bifurcation occurs, only one representative nodal domain triple is shown for each of the solution curve segments. In Figs. 4 and 6, the plots of the nodal domains (in the form of squared sums) overlap to show their relative positions. The corresponding triples and overlapping nodal domains are labeled by the same capital letters in different figures, e.g. Figs. 3 and 4.

Now, we justify the continuation parameter-switching scheme and note some observations from the numerical results shown in the figures.

1. In Step (ii) of Algorithm 3, we follow the solution curve $\mathcal{C}_1$ by increasing β from 0 to 0.2. As the initial solution $(\bar{\mathbf{u}}, \bar{\mathbf{u}}, \bar{\mathbf{u}})$ is the global (thus also local) minimal energy solution, and there is no bifurcation found in the interval $0 \leqslant \beta \leqslant 0.2$, the states of the solutions are thus unchanged by Theorem 10. That is, all the intermediate solutions are all local minimal solutions corresponding to each of the β's. Furthermore, we anticipate that all these solutions corresponding to each of the β's are ground state solutions, due to the following observation. In this setting, all the interactions are attractive. Consequently, the three components tend to gather together and concentrate at the center of the domain to achieve minimal energy. Such solution profiles are similar to the solution profile of the initial solution $(\bar{\mathbf{u}}, \bar{\mathbf{u}}, \bar{\mathbf{u}})$ for $\beta = 0$. It is thus reasonable that $(\bar{\mathbf{u}}, \bar{\mathbf{u}}, \bar{\mathbf{u}})$ is a good initial guess for the global minimal solution of a DNLS with a small positive β. By using the continuation method, we thus can track the global minimal solutions in $\mathcal{C}_1$.
2. The curve $\mathcal{C}_2$ acts as a "bridge" connecting the two settings in Step (ii) and Step (iv) Algorithm 3. In particular, δ_{23} is changed from 1 (three attractive interactions) to -1 (one repulsive and two attractive interactions). Fig. 3 shows that there is only one bifurcation point in $\mathcal{C}_2$, where $\delta_{23} = -0.314$. At this bifurcation point, METCM suggests tracking either the upper

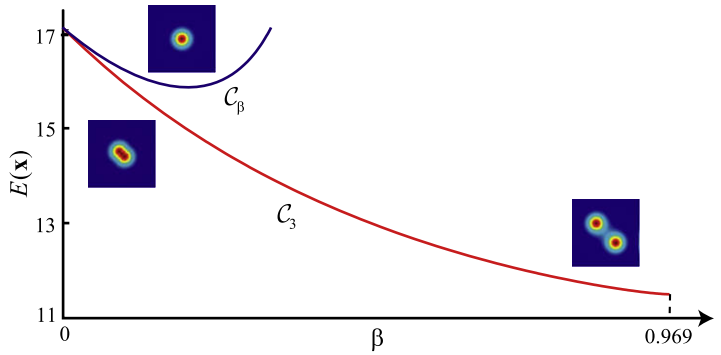

Fig. 7. Compared with $\mathcal{C}_\beta$, the solution curve $\mathcal{C}_3$ has lower energies.

or the lower bifurcation branch (the red[1] curves) to retain minimal energy solutions. By tracking either one of the branches, non-radially symmetric solutions are observed. Furthermore, as shown in Fig. 4, the solutions of these bifurcation branches have lower energies than the ones on the primal stalk of $\mathcal{C}_2$ (the blue curve).

3. In Step (iv) of Algorithm 3, we switch to the target setting, in which one repulsive and two attractive interactions are assumed. We use the non-radially symmetric solution obtained in the terminal point of $\mathcal{C}_2$, in which $\delta_{23} = -1$, as the initial guess for tracking the curve $\mathcal{C}_3$. If we decrease β from 0.2 to 0^+, the target non-radially symmetric solutions are obtained while β approaches zero. As shown in Fig. 5, no bifurcation occurs for $0 < \beta \leqslant 0.2$, so all the computed solutions remain minimal energy solutions. Consequently, we find the non-radially symmetric solution for one repulsive and two attractive interactions with small β.

In short, we have shown how the parameter-switching scheme can lead to the non-radially symmetric solution predicted in [20]. These non-radially symmetric positive solutions are expected to be the ground state solutions of (38). This conjecture is based on the following observations. We start from the ground state solution for $\beta = 0$ and then track $\mathcal{C}_1$ until $\beta = 0.2$. We then track the path with lower energy solutions in $\mathcal{C}_2$, when the only bifurcation occurs, and obtain non-radially symmetric solutions. As there is no other bifurcation point in $\mathcal{C}_3$, the value for β changes from 0.2 to 0^+. The ground state character of the initial solutions is preserved in the tracked non-radially symmetric solutions.

Finally, we make the following remarks on the numerical experiments.

Remark 3. We can also track the primal stalk of $\mathcal{C}_2$ in Step (iii) of Algorithm 3 until $\delta_{23} = -1$ (i.e. the blue curve in Fig. 3), and then track $\mathcal{C}_\beta$ by decreasing $\beta = 0.2$ to 0^+. However, we would only find radially symmetric solutions, whose energies are higher than those of the non-radially symmetric solutions we have found.

Remark 4. In Fig. 7, we compare the energy curves of $\mathcal{C}_3$ and $\mathcal{C}_\beta$. The energy curve of $\mathcal{C}_3$ is lower than that of $\mathcal{C}_\beta$. This result is obviously consistent with the consequence reported in [20].

Remark 5. Another type of non-radially symmetric positive solution can be found by following the solution curve $\mathcal{C}_3$ and increasing the values of β from 0.2 to 1^-. A representative of such solutions is shown in Fig. 5 for $\beta \approx 0.969$.

5. Conclusion

This article focused on the use of continuation methods to solve the time-independent m-component discrete nonlinear Schrödinger equations. In particular, we propose a new algorithm that is capable of tracking the local minimal energy solutions along the solution curves. We have also shown how we may compute the ground states of the decoupled discrete nonlinear Schrödinger equation with $V(\mathbf{z}) = 0$. By combining these two techniques with a parameter-switching scheme, we find non-radially symmetric minimal energy solutions for the case with one repulsive and two attractive interactions and small coupling coefficients.

We believe our minimal energy tracking continuation method can be applied to other coupled elliptic partial differential equations, probably with suitable modifications. The method thus acts as a useful tool for exploring various steady-state solutions of the differential equations.

Acknowledgments

The authors are grateful to the anonymous referees for their valuable and helpful comments and suggestions. This work is partially supported by the National Science Council, the National Center for Theoretical Sciences, and the Taida Institute of Mathematical Sciences in Taiwan.

[1] For interpretation of color in Fig. 3, the reader is referred to the web version of this article.

Appendix A

A.1. Proof of Theorem 1

Eqs. (12) and (13) imply that $\mathbf{f}$ is continuous on $\mathcal{M}$. By the definition of (11), $\mathcal{M}$ is homeomorphic to an $(N-1)$-dimensional standard simplex, which is convex and compact. Applying the Schauder fixed point theorem to $\mathbf{f}$, we can see that there is a point $\mathbf{u}^* \in \mathcal{M}$ satisfying

$$\mathbf{f}(\mathbf{u}^*) = \mathbf{u}^*. \tag{39}$$

The existence of the fixed point $\mathbf{u}^* \in \mathring{\mathcal{M}}$ follows from the fact that the function $\mathbf{f}$ in (13) maps $\mathcal{M}$ into $\mathring{\mathcal{M}}$. From (10), (13) and (39), we have

$$\|\overline{\mathbf{A}}^{-1}\mathbf{u}^{*③}\|_4^{-1}\mathbf{u}^{*③} = (\lambda\mathbf{I} - \mathbf{A})\mathbf{u}^*. \tag{40}$$

Multiplying (40) by $\frac{1}{\mu^{1/2}}\|\overline{\mathbf{A}}^{-1}\mathbf{u}^{*③}\|_4^{-1/2}$ from the left and setting

$$\bar{\mathbf{u}}(\mu) = \frac{1}{\mu^{1/2}}\|\overline{\mathbf{A}}^{-1}\mathbf{u}^{*③}\|_4^{-1/2}\mathbf{u}^*,$$

we obtain

$$\mathbf{A}\bar{\mathbf{u}}(\mu) - \lambda\bar{\mathbf{u}}(\mu) + \mu\bar{\mathbf{u}}(\mu)^③ = \mathbf{0}.$$

It is easy to verify that $\bar{\mathbf{u}}(\mu)$ belongs to $\mathcal{N}_1$. This completes the proof. □

A.2. Proof of Theorem 2

(i) Since $\mathbf{u}, \mathbf{v} \in \mathcal{M}$, we have $\|\mathbf{u}\|_4 = 1, \|\mathbf{v}\|_4 = 1$ and

$$\widehat{E}(\mathbf{v}) = \mathbf{v}^\top(\lambda\mathbf{I} - \mathbf{A})\mathbf{v}. \tag{41}$$

Substituting $\mathbf{v} = \mathbf{f}(\mathbf{u}) = \frac{\overline{\mathbf{A}}^{-1}\mathbf{u}^③}{\|\overline{\mathbf{A}}^{-1}\mathbf{u}^③\|_4}$ into (41), we get

$$\widehat{E}(\mathbf{v}) = \mathbf{v}^\top(\lambda\mathbf{I} - \mathbf{A})\mathbf{v} = \frac{1}{\|\overline{\mathbf{A}}^{-1}\mathbf{u}^③\|_4}\mathbf{v}^\top\mathbf{u}^③.$$

Letting $c = \frac{1}{\|\overline{\mathbf{A}}^{-1}\mathbf{u}^③\|_4}$ and applying the Hölder inequality ($|\mathbf{x}^\top\mathbf{y}| \leqslant \|\mathbf{x}\|_p\|\mathbf{y}\|_q$ where $\frac{1}{p} + \frac{1}{q} = 1$ and $p > 1$) with $p = 4, q = 4/3, \mathbf{x} = \mathbf{v}$ and $\mathbf{y} = \mathbf{u}^③$, we obtain

$$\mathbf{v}^\top(\lambda\mathbf{I} - \mathbf{A})\mathbf{v} \leqslant c\|\mathbf{v}\|_4\|\mathbf{u}\|_4^3 = c. \tag{42}$$

Since $\|\mathbf{u}\|_4 = 1$, we have

$$c = \frac{\mathbf{u}^\top\overline{\mathbf{A}\mathbf{A}}^{-1}\mathbf{u}^③}{\|\overline{\mathbf{A}}^{-1}\mathbf{u}^③\|_4} = \mathbf{u}^\top(\lambda\mathbf{I} - \mathbf{A})\mathbf{v}. \tag{43}$$

Since $\lambda\mathbf{I} - \mathbf{A}$ is positive definite, it has the Cholesky factorization $(\lambda\mathbf{I} - \mathbf{A}) = \mathbf{L}^\top\mathbf{L}$. Applying the Cauchy-Schwarz inequality to (43), we obtain

$$c = \mathbf{u}^\top\mathbf{L}^\top\mathbf{L}\mathbf{v} \leqslant \sqrt{\mathbf{u}^\top\mathbf{L}^\top\mathbf{L}\mathbf{u}} \cdot \sqrt{\mathbf{v}^\top\mathbf{L}^\top\mathbf{L}\mathbf{v}} = \sqrt{\mathbf{u}^\top(\lambda\mathbf{I} - \mathbf{A})\mathbf{u}} \cdot \sqrt{\mathbf{v}^\top(\lambda\mathbf{I} - \mathbf{A})\mathbf{v}}. \tag{44}$$

From (42) and (44), it follows that

$$\mathbf{v}^\top(\lambda\mathbf{I} - \mathbf{A})\mathbf{v} \leqslant c \leqslant \sqrt{\mathbf{u}^\top(\lambda\mathbf{I} - \mathbf{A})\mathbf{u}} \cdot \sqrt{\mathbf{v}^\top(\lambda\mathbf{I} - \mathbf{A})\mathbf{v}} \tag{45}$$

and therefore

$$\sqrt{\mathbf{v}^\top(\lambda\mathbf{I} - \mathbf{A})\mathbf{v}} \leqslant \sqrt{\mathbf{u}^\top(\lambda\mathbf{I} - \mathbf{A})\mathbf{u}}.$$

Using the fact that $\|\mathbf{v}\|_4 = \|\mathbf{u}\|_4 = 1$, we have

$$\widehat{E}(\mathbf{v}) = \frac{\mathbf{v}^\top(\lambda\mathbf{I} - \mathbf{A})\mathbf{v}}{\|\mathbf{v}\|_4^2} \leqslant \frac{\mathbf{u}^\top(\lambda\mathbf{I} - \mathbf{A})\mathbf{u}}{\|\mathbf{u}\|_4^2} = \widehat{E}(\mathbf{u}). \tag{46}$$

The equality in (46) holds if and only if the inequalities in (42) and (44) become equalities. Furthermore, both inequalities in (42) and (44) hold if and only if the vectors $\mathbf{v}$ and $\mathbf{u}$ are linearly dependent, i.e. $\mathbf{v} = a\mathbf{u}$ for some $a \in \mathbb{R}$. Since $\mathbf{v} > 0, \mathbf{u} > 0$ with $\|\mathbf{v}\|_4 = \|\mathbf{u}\|_4 = 1$, we have $\mathbf{v} = \mathbf{u}$. Hence, the equality in (46) holds if and only if $\mathbf{u}$ is a fixed point of $\mathbf{f}$.

(ii) Since the sequence $\{\mathbf{u}_i\}_{i=0}^\infty \subset \mathcal{M}$ is bounded, there exists a convergent subsequence $\{\mathbf{u}_{n_i}\}_{i=0}^\infty$ and a point $\mathbf{u}^* \in \mathcal{M}$ such that

$$\lim_{i\to\infty}\mathbf{u}_{n_i} = \mathbf{u}^*.$$

Consequently, we have

$$\lim_{i\to\infty}\widehat{E}(\mathbf{u}_{n_i})=\widehat{E}(\mathbf{u}^*)\ \text{and}\ \lim_{i\to\infty}\widehat{E}(\mathbf{f}(\mathbf{u}_{n_i}))=\widehat{E}(\mathbf{f}(\mathbf{u}^*)), \tag{47}$$

as $\mathbf{f}$ and $\widehat{E}$ are continuous. Furthermore, since the cost function $\widehat{E}(\cdot)$ in (9b) is continuous on the compact set $\mathcal{M}$, the function $\widehat{E}(\cdot):\mathcal{M}\to\mathbb{R}_+$ attains its minimum value on $\mathcal{M}$. From part (i) of this theorem, it can be easily seen that the sequence $\{\widehat{E}(\mathbf{u}_i)\}_{i=1}^{\infty}$ converges to a certain positive number $\widehat{E}^*$. That is,

$$\lim_{i\to\infty}\widehat{E}(\mathbf{u}_i)=\widehat{E}^*. \tag{48}$$

By Eqs. (47) and (48), and the fact that $\{\widehat{E}(\mathbf{u}_{n_i})\}_{i=0}^{\infty}$ and $\{\widehat{E}(\mathbf{f}(\mathbf{u}_{n_i}))\}_{i=0}^{\infty}$ are subsequences of $\{\widehat{E}(\mathbf{u}_i)\}_{i=0}^{\infty}$, we see that the three sequences converge to the same value. Consequently, we have

$$\widehat{E}(\mathbf{f}(\mathbf{u}^*))=\widehat{E}(\mathbf{u}^*).$$

By part (i) of this theorem, we conclude that $\mathbf{f}(\mathbf{u}^*)=\mathbf{u}^*$. □

A.3. Proof of Lemma 4

By definition,

$$\|\mathbf{u}_{i+1}-\mathbf{u}_i\|_{\overline{\mathbf{A}}}^2=(\mathbf{u}_{i+1}-\mathbf{u}_i)^{\top}\overline{\mathbf{A}}(\mathbf{u}_{i+1}-\mathbf{u}_i)=\mathbf{u}_{i+1}^{\top}\overline{\mathbf{A}}\mathbf{u}_{i+1}+\mathbf{u}_i^{\top}\overline{\mathbf{A}}\mathbf{u}_i-2\mathbf{u}_{i+1}^{\top}\overline{\mathbf{A}}\mathbf{u}_i=\widehat{E}(\mathbf{u}_{i+1})+\widehat{E}(\mathbf{u}_i)-2\mathbf{u}_{i+1}^{\top}\overline{\mathbf{A}}\mathbf{u}_i. \tag{49}$$

From (42), (43) and (45), we have

$$\widehat{E}(\mathbf{u}_{i+1})\leqslant\mathbf{u}_{i+1}^{\top}\overline{\mathbf{A}}\mathbf{u}_i\leqslant\sqrt{\widehat{E}(\mathbf{u}_{i+1})}\sqrt{\widehat{E}(\mathbf{u}_i)}. \tag{50}$$

Furthermore, by (49) and (50), it follows that

$$\|\mathbf{u}_{i+1}-\mathbf{u}_i\|_{\overline{\mathbf{A}}}\leqslant\sqrt{\widehat{E}(\mathbf{u}_i)-\widehat{E}(\mathbf{u}_{i+1})}, \tag{51}$$

or equivalently, $\lim_{i\to\infty}\|\mathbf{u}_{i+1}-\mathbf{u}_i\|_{\overline{\mathbf{A}}}=0$. □

A.4. Proof of Theorem 5

Since $\mathbf{u}^*$ is a strictly local minimum of the optimization problem (9), the Hessian matrix $\mathbf{H}(\mathbf{u}^*)$ of $\widehat{E}(\mathbf{u})$ is positive definite. Therefore, there is a $\delta>0$ such that $\mathbf{H}(\mathbf{u})$ is positive definite, i.e. $\widehat{E}(\mathbf{u})$ is convex, for $\mathbf{u}\in\mathcal{M}$ and $\|\mathbf{u}-\mathbf{u}^*\|_{\overline{\mathbf{A}}}<\delta$.

For any positive number $0<\varepsilon<\delta/2$, we let

$$\widehat{E}_{\varepsilon}=\min_{\|\mathbf{u}-\mathbf{u}^*\|_{\overline{\mathbf{A}}}=\varepsilon}\widehat{E}(\mathbf{u})>\widehat{E}^*, \tag{52}$$

where $\widehat{E}^*$ is given by (48), and define

$$B(\mathbf{u}^*,\widehat{E}_{\varepsilon})=\left\{\mathbf{u}\in\mathcal{M}\,\middle|\,\|\mathbf{u}-\mathbf{u}^*\|_{\overline{\mathbf{A}}}<\varepsilon,\ \widehat{E}(\mathbf{u})<\widehat{E}_{\varepsilon}\right\}. \tag{53}$$

From (15) and (16), there exists $N_0\in\mathbb{N}$ such that

$$\mathbf{u}_{n_j}\in B(\mathbf{u}^*,\widehat{E}_{\varepsilon})\ \text{and}\ \|\mathbf{u}_{i+1}-\mathbf{u}_i\|_{\overline{\mathbf{A}}}<\varepsilon\ \text{for}\ n_j,\ i>N_0. \tag{54}$$

Since $2\varepsilon<\delta$, if $\mathbf{u}_i\in B(\mathbf{u}^*,\widehat{E}_{\varepsilon})$ and $\|\mathbf{u}_{i+1}-\mathbf{u}_i\|_{\overline{\mathbf{A}}}<\varepsilon$, then $\|\mathbf{u}_{i+1}-\mathbf{u}^*\|_{\overline{\mathbf{A}}}<2\varepsilon$. On the other hand, using the fact that $\widehat{E}(\mathbf{u}_{i+1})\leqslant\widehat{E}(\mathbf{u}_i)<\widehat{E}_{\varepsilon}$ and $\widehat{E}(\mathbf{u})$ is convex on $\|\mathbf{u}-\mathbf{u}^*\|_{\overline{\mathbf{A}}}<\delta$ it holds that $\mathbf{u}_{i+1}\in B(\mathbf{u}^*,\widehat{E}_{\varepsilon})$. Thus, we have

$$\|\mathbf{u}_i-\mathbf{u}^*\|_{\overline{\mathbf{A}}}<\varepsilon\ \text{for all}\ i>N_0.$$

This completes the proof. □

A.5. Proof of Lemma 8

Since $\mathbf{y}^*=(\mathbf{x}^{*\top},\beta^*)^{\top}$ is a bifurcation point, the matrix $\mathbf{G}_{\mathbf{x}}(\mathbf{y}^*)$ is singular. Thus there exists a nonzero vector $\mathbf{z}=(\mathbf{z}_1^{\top},\ldots,\mathbf{z}_m^{\top})^{\top}\in\mathbb{R}^{mN}$ such that

$$\mathbf{G}_{\mathbf{x}}(\mathbf{y}^*)\mathbf{z}=\mathbf{0}. \tag{55}$$

Now, we claim that $\nabla\mathbf{g}(\mathbf{x}^*)\mathbf{z}=\mathbf{0}$. Since $\mathbf{y}^*$ is a solution of DNLS Eq. (21) and $\mathbf{x}^*=(\mathbf{u}_1^{*\top},\ldots,\mathbf{u}_m^{*\top})^{\top}$, the vector $\nabla g_j(\mathbf{x}^*)$ in (31) can be written as

$$\nabla g_j(\mathbf{x}^*)^\top = \begin{bmatrix} 2\beta_{1j}\mathbf{u}_1^* \circ \mathbf{u}_j^{*②} \\ \vdots \\ 2\beta_{(j-1)j}\mathbf{u}_{j-1}^* \circ \mathbf{u}_j^{*②} \\ 2\mu_j\mathbf{u}_j^* \circ \mathbf{u}_j^{*②} \\ 2\beta_{(j+1)j}\mathbf{u}_{j+1}^* \circ \mathbf{u}_j^{*②} \\ \vdots \\ 2\beta_{mj}\mathbf{u}_m^* \circ \mathbf{u}_j^{*②} \end{bmatrix} \in \mathbb{R}^{mN}, \tag{56}$$

for $j = 1, 2, \ldots, m$. Let

$$\mathbf{U}(\mathbf{x}^*) = \begin{pmatrix} \mathbf{u}_1^* & \mathbf{0} & \cdots & \mathbf{0} \\ \mathbf{0} & \mathbf{u}_2^* & \ddots & \mathbf{0} \\ \vdots & \vdots & \ddots & \mathbf{0} \\ \mathbf{0} & \cdots & \cdots & \mathbf{u}_m^* \end{pmatrix} \in \mathbb{R}^{mN\times m}. \tag{57}$$

A calculation leads to

$$\mathbf{U}(\mathbf{x}^*)^\top \mathbf{G}_{\mathbf{x}}(\mathbf{y}^*) = \nabla \mathbf{g}(\mathbf{x}^*). \tag{58}$$

From (55) and (58), it is easy to verify that $\nabla \mathbf{g}(\mathbf{x}^*)\mathbf{z} = \mathbf{0}$, that is, there exists a nonzero vector $\bar{\mathbf{z}} \in \mathbb{R}^{\ell}$ such that $\mathbf{z} = \mathbf{P}(\mathbf{x}^*)\bar{\mathbf{z}}$. Hence, from (34), we obtain $\mathbf{H}(\mathbf{y}^*)\bar{\mathbf{z}} = \mathbf{0}$, i.e. $\det(\mathbf{H}(\mathbf{y}^*)) = 0$.

A.6. Proof of Lemma 9

First, we note that from (36), (57), (58) and (59), we have

$$\mathbf{U}(\mathbf{x})^\top \mathbf{G}_{\mathbf{x}}(\mathbf{y})\mathbf{U}(\mathbf{x}) = \mathbf{\Sigma}(\mathbf{y}), \tag{59}$$

for each $\mathbf{y} = (\mathbf{x}^\top, \beta)^\top \in \mathcal{C}$.

Since $\mathbf{y}^* = (\mathbf{x}^{*\top}, \beta^*)^\top \in \mathcal{C}$ and $\det(\mathbf{H}(\mathbf{y}^*)) = 0$, there exists a nonzero vector $\bar{\mathbf{z}} \in \mathbb{R}^{mN-m}$ such that

$$\mathbf{H}(\mathbf{y}^*)\bar{\mathbf{z}} = \mathbf{0}. \tag{60}$$

Let $\mathbf{z} = \mathbf{P}(\mathbf{x}^*)\bar{\mathbf{z}} \in \mathbb{R}^{mN}$. Note that $\mathbf{z}$ is a nonzero vector, since $\mathbf{P}(\mathbf{x}^*)$ is of full column rank. Now we claim that $\mathbf{G}_{\mathbf{x}}(\mathbf{y}^*)\mathbf{z} = \mathbf{0}$. From (59) and (58), it follows that

$$\mathbf{U}(\mathbf{x}^*)^\top \mathbf{G}_{\mathbf{x}}(\mathbf{y}^*)\mathbf{z} = \nabla \mathbf{g}(\mathbf{x}^*)\mathbf{z} = \mathbf{0}. \tag{61}$$

On the other hand, from (34) and (60) we have

$$\mathbf{P}(\mathbf{x}^*)^\top \mathbf{G}_{\mathbf{x}}(\mathbf{y}^*)\mathbf{z} = \mathbf{0}. \tag{62}$$

Combing (61) and (62) gives

$$\begin{bmatrix} \mathbf{P}(\mathbf{x}^*)^\top \\ \mathbf{U}(\mathbf{x}^*)^\top \end{bmatrix} \mathbf{G}_{\mathbf{x}}(\mathbf{y}^*)\mathbf{z} = \mathbf{0}. \tag{63}$$

We calculate that

$$\begin{bmatrix} \mathbf{P}(\mathbf{x}^*)^\top \\ \nabla \mathbf{g}(\mathbf{x}^*) \end{bmatrix} [\mathbf{P}(\mathbf{x}^*), \mathbf{U}(\mathbf{x}^*)] = \begin{bmatrix} \mathbf{I}_{m(N-1)} & \mathbf{P}(\mathbf{x}^*)^\top \mathbf{U}(\mathbf{x}^*) \\ \mathbf{0} & \mathbf{\Sigma}(\mathbf{x}^*) \end{bmatrix}. \tag{64}$$

Here, the (1,1) entry in (64) follows from the fact that the column vectors of $\mathbf{P}(\mathbf{x}^*)$ are orthonormal, the (2,1) entry follows from Eq. (35) and the (2,2) entry follows from Eqs. (58) and (59). Since $\mathbf{\Sigma}(\mathbf{y}^*)$ is invertible, it follows that the $mN \times mN$ matrix $[\mathbf{P}(\mathbf{x}^*), \mathbf{U}(\mathbf{x}^*)]$ is invertible. From (63), we obtain $\mathbf{G}_{\mathbf{x}}(\mathbf{y}^*)\mathbf{z} = \mathbf{0}$, that is, $\det(\mathbf{G}_{\mathbf{x}}(\mathbf{y}^*)) = 0$.

References

[1] N. Akhmediev, A. Ankiewicz, Partially coherent solitons on a finite background, Phys. Rev. Lett. 82 (1999) 2661–2664.
[2] E.L. Allgother, K. Gerog, Numerical path following, in: P.G. Ciarlet, J.L. Lions (Eds.), Handbook of Numerical Analysis, vol. V, Elsevier, 1997.
[3] D. Bambusi, A. Sacchetti, Exponential times in the one-dimensional Gross–Pitaevskii equation with multiple well potential, Commun. Math. Phys. 275 (1) (2007) 1–36.
[4] W.-Z. Bao, Ground states and dynamics of multi-component Bose–Einstein condensates, SIAM Multisc. Model. Simul. 2 (2) (2004) 210–236.

[5] W.-Z. Bao, Q. Du, Computing the ground state solution of Bose–Einstein condensates by a normalized gradient flow, SIAM J. Sci. Comput. 25 (5) (2004) 1674–1697.
[6] F.S. Cataliotti, S. Burger, C. Fort, P. Maddaloni, F. Minardi, A. Trombettoni, A. Smerzi, M. Inguscio, Josephson junction arrays with Bose–Einstein condensates, Science 293 (2001) 843.
[7] S.-L. Chang, C.-S. Chien, B.-W. Jeng, Liapunov–Schmidt reduction and continuation for nonlinear Schrödinger equations, SIAM J. Sci. Comput. 27 (2007) 729–755.
[8] S.-M. Chang, Y.-C. Kuo, W.-W. Lin, S.-F. Shieh, A continuation BSOR-Lanczos–Galerkin method for positive bound states of a multi-component Bose–Einstein condensate, J. Comp. Phys. 210 (2005) 439–458.
[9] S.-M. Chang, W.-W. Lin, S.-F. Shieh, Gauss–Seidel-type methods for energy states of a multi-component Bose–Einstein condensate, J. Comp. Phys. 202 (2005) 367–390.
[10] K.W. Chow, Periodic solutions for a system of four coupled nonlinear Schrödinger equations, Phys. Lett. A 285 (2001) 319–326.
[11] D.N. Christodoulides, R.I. Joseph, Discrete self-focusing in nonlinear arrays of coupled waveguides, Opt. Lett. 13 (9) (1988) 794.
[12] D.N. Christodoulides, F. Lederer, Y. Silberberg, Discretizing light behaviour in linear and nonlinear waveguide lattices, Nature 424 (2003) 817–823.
[13] A.S. Davydov, The theory of contraction of proteins under their excitation, J. Theor. Biol. 38 (3) (1973) 559–569. March.
[14] F.T. Hioe, Solitary waves for n coupled nonlinear Schrödinger equations, Phys. Rev. Lett. 82 (1999) 1152–1155.
[15] F.T. Hioe, T.S. Salter, Special set and solutions of coupled nonlinear Schrödinger equations, J. Phys. A: Math. Gen. 35 (2002) 8913–8928.
[16] T. Kanna, M. Lakshmanan, Exact soliton solutions shape changing collisions and partially coherent solitons in coupled nonlinear Schrödinger equations, Phys. Rev. Lett. 86 (2001) 5043–5046.
[17] H.B. Keller, Lectures on Numerical Methods in Bifurcation Problems, Springer-Verlag, Berlin, 1987.
[18] Y.-C. Kuo, W.-W. Lin, S.-F. Shieh, W. Wang, A hyperplane-constrained continuation method for near singularity in coupled nonlinear Schrödinger equations, Preprint, 2008.
[19] M.K. Kwong, Uniqueness of positive solutions of $\Delta u - u + u^p = 0$ in R^n, Arch. Rational Mech. Anal 105 (3) (1989) 243–266.
[20] T.-C. Lin, J. Wei, Ground state of n coupled nonlinear Schrödinger equations in $\mathbb{R}^n$, $n \leqslant 3$, Commun. Math. Phys. 255 (2005) 629–653.
[21] M. Mitchell, Z. Chen, M. Shih, M. Segev, Self-trapping of partially spatially incoherent light, Phys. Rev. Lett. 77 (1996) 490–493.
[22] J. Nocedal, S. Wright, Numerical Optimization, second ed., Springer, 2006.
[23] A. Trombettoni, A. Smerzi, Discrete solitons and breathers with dilute Bose–Einstein condensates, Phys. Rev. Lett. 86 (2001) 2353–2356.
[24] A. Trombettoni, A. Smerzi, A.R. Bishop, Discrete nonlinear Schrödinger equation with defects, Phys. Rev. E 67 (1) (2003) 016607.